



FluidFlower Benchmark: Lessons Learned from the Perspective of Subsurface Simulation

Michiel Wapperom¹ · Xiaoming Tian¹ · Aleks Novikov¹ · Denis Voskov^{1,2}

Received: 13 January 2023 / Accepted: 24 June 2023 / Published online: 17 July 2023
© The Author(s) 2023

Abstract

In this work, we describe our decisions made to perform the FluidFlower simulation study and discuss various aspects of the benchmark that are different from our usual subsurface simulation practice. We will discuss the impact of various modeling choices on the outcomes of the simulation models, such as gridding, discretization, and solver strategies, and the lessons learned, taking into account the different conditions of the FluidFlower study compared to conditions commonly dealt with in subsurface simulation. We will start with a brief description of the DARTS framework utilized for compositional simulation, the thermodynamic and physical modeling related to the atmospheric CO₂-brine system, and the modeling workflow used in our benchmark submission. Additionally, we describe a custom nonlinear solver developed for the atmospheric benchmark conditions to improve convergence including the linear solver strategy since our default two-stage preconditioner does not perform effectively. To make meaningful comparisons between each of the modeling choices, we define a baseline model which is a simplified version of our setup in the main FluidFlower benchmark. The baseline model is then used to study the effect of Cartesian and unstructured meshes and a two-point flux approximation compared with a multi-point flux approximation for capturing the physics at play. We conclude our work with lessons learned and future recommendations.

Keywords FluidFlower · CCUS · Operator-based linearization · Unstructured grids · TPFA · MPFA · Linear solver

1 Introduction

The development of methods for geological sequestration of CO₂ is of major importance toward realizing lower levels of atmospheric greenhouse gases. In modeled pathways that limit global warming to 2 °C, the cumulative global amount of 170–900 GtCO₂ is

✉ Denis Voskov
d.v.voskov@tudelft.nl

Michiel Wapperom
m.b.wapperom@tudelft.nl

¹ Department of Geoscience and Engineering, Delft University of Technology, Delft, Netherlands

² Department of Energy Resources Engineering, Stanford University, Stanford, CA, USA

accounted for geological sequestration over 2020–2100 (Shukla et al. 2017). Permanent subsurface storage of CO₂ relies on a range of trapping mechanisms, which involve different physical aspects related to the characteristics of reservoirs and fluids: structural trapping (Ajayi et al. 2019; Ringrose 2020), residual trapping of immobile free gas CO₂ due to capillary forces, dissolution trapping in brine and mineral trapping (Pruess and Nordbotten 2011; Fan et al. 2012; Delshad et al. 2013).

The dynamic behavior of the CO₂ plume in sequestration processes involves buoyancy-driven convective migration, chemical interactions, diffusion of CO₂ with brine, reservoir heterogeneity, and chemical rock alteration. Several analytical models and semi-analytical approaches were developed to quantify some of these effects (Nordbotten and Celia 2006; Hesse et al. 2008; Juanes et al. 2010). Riaz and Tchelepi (2004) presented the analysis based on perturbation theory, which predicts the convective instability of dissolved CO₂ and enhanced dissolution rates for a small-scale homogeneous domain. This model was further improved and validated against experimental results in Neufeld et al. (2010). Another attempt to connect simulation with experiments has been performed in Farajzadeh et al. (2009). Subsequently, the analytical model was enhanced to account for capillary transition effects (Elenius et al. 2014), realistic density (Nomeli et al. 2014), and viscosity variations (Daniel and Riaz 2014). Moreover, the influence of a simplified layer cake heterogeneity was addressed in Ghorbani et al. (2017).

These models attempt to address the important geological and residual trapping mechanisms linked to CO₂ sequestration at relatively short time scales after injection (tens to hundreds of years) but have been hampered to date by the lack of geologically realistic input models that capture key heterogeneities of interest across length-scales. Furthermore, it is infeasible that any combined analytical model will be capable of representing all phenomena together for a range of realistic parameters relevant to industrial CO₂ sequestration projects with realistic geological heterogeneity. Numerical modeling is essential for such representation. At longer time scales (hundreds to thousands of years), however, numerical models, too, only approximately represent the dissolution trapping that dominates in the reservoir. This is a concern given the discrepancies between different modern simulation approaches, as reported in the benchmark study by Nordbotten et al. (2012). This benchmark study also illustrates the high sensitivity of the existing models to the physical assumptions even under conditions of simplified geological properties.

Several numerical models covering the enhanced dissolution of CO₂ in brine have been proposed in the literature. Riaz et al. (2006) introduced an enhanced dissolution model in a small domain (a few tens of meters) to validate analytical results. This model is based on a high-order approximation and applied to a wide range of Rayleigh numbers. Pau et al. (2010) and Farajzadeh et al. (2011) demonstrate convective dissolution studied in homogeneous 2D and 3D small domains based on a conventional finite-volume scheme. More recently, this analysis was extended for hysteretic systems (Wang et al. 2022). Elenius and Gasda (2013) investigated how horizontal barriers affect the convective mixing of CO₂. Elenius et al. (2015) present numerically converged solutions for a small 2D domain with a different type of capillary transition zone validated against analytical solutions. For the first time, they obtain a numerically converged solution for a large-scale plume migration problem with a wide range of dominant physical phenomena. Later, the same simulation framework has been extended for more advanced thermodynamics treatment with chemistry (Voskov et al. 2017).

An attempt to assess the predictive capabilities of simulation models has been made in the FluidFlower benchmark study (Flemish et al. 2023). In the study, a modeling benchmark for CO₂ sequestration was created based on physical experiments, although conducted at

atmospheric conditions. A small-scale heterogeneous geometry based on typical North Sea reservoirs was constructed in a meter-scale rig, filled with unconsolidated sands of different sand types (Nordbotten et al. 2022). CO₂ was injected into the system for a few hours, and the evolution of the CO₂ plume throughout the reservoir was recorded over several days. Numerical simulation groups were provided with geometrical, petrophysical, and operational information. The reported forecasts from numerical simulation groups could be analyzed in the presence of physical ground truth, provided by a series of repeated physical experiments on the experimental rig. Numerical models have been able to capture the relevant physical processes with reasonable accuracy. However, the limited nature of the information provided in this benchmark study and the unfamiliar simulation conditions under which the experiments were conducted, presented a wide range of modeling decisions and raised a number of relevant questions from the perspective of subsurface simulation. Faced with time constraints, many decisions could not be thoroughly addressed during the blind phase of the benchmark study.

In hindsight and with knowledge of the results of the physical experiments, we can reflect on decisions and issues regarding physical and numerical modeling. The aim of this study is to address the questions that arose during our attempts in the main benchmark study, examine the effects of different modeling choices and relate our findings in the benchmark to experiences in subsurface simulation. We will start with a brief description of our open-source DARTS simulation framework and the predictive modeling workflow utilized in the benchmark study. Then, we describe the time-step heuristics used for the conditions of the benchmark, followed by a discussion of linear solver strategies. Following up, the impact of modeling decisions regarding grid structure and resolution will be examined, as well as a comparison between two-point and multi-point flux approximations. Some of the issues encountered here originate from the contrast between reservoir and benchmark conditions. We will illustrate this difference in results and performance and draw the lessons learned from the perspective of reservoir simulation.

2 Methodology

In this section, an outline of the DARTS submission to the FluidFlower benchmark is given. The description guides the reader through the modeling choices that we made. First, the assumptions made in the physical modeling of the system at atmospheric conditions are described, as well as the choices for modeling the most representative physics with sufficient accuracy in a reasonable time. Following this, a baseline model is developed from which the effect of different numerical modeling choices can be investigated.

The FluidFlower study considers the injection of CO₂ into brine-saturated formations close to atmospheric conditions. The dominating trapping mechanisms under these conditions rely to a large extent on capillary effects and properties related to a mutual dissolution of CO₂ and water: solubility, density differences, and diffusion. The accuracy of the modeling of these physical phenomena and the corresponding computational grid determines to what extent the dynamics of the FluidFlower can be captured in simulation.

2.1 Mathematical Model

In our mathematical model of the FluidFlower setup, we used a compositional formulation under isothermal conditions. The system of equations describing such formulation can be written in the following form

$$\frac{\partial}{\partial t} \int_{\Omega} M^c d\Omega + \int_{\Gamma} \mathbf{F}^c \cdot \mathbf{n} d\Gamma = 0, \quad (1)$$

where Ω is the control volume, Γ is the interface, M^c is the accumulation term for the c^{th} component ($c = 1, \dots, n_c$, index of the mass components; for the benchmark it is water and CO_2), \mathbf{F}^c is the flux term of the c^{th} component and \mathbf{n} is the unit normal direction pointing outward to the domain boundary.

The accumulation term M^c for a given component c is written as:

$$M^c = \phi \sum_{j=1}^{n_p} x_{cj} \rho_j s_j, \quad c = 1, \dots, n_c, \quad (2)$$

where ϕ is porosity, s_j is the saturation of phase j , ρ_j is the density (kmol/m^3) of phase j , and x_{cj} is the molar fraction of component c in phase j .

The mass flux of each component is represented by the summation over n_p fluid phases,

$$\mathbf{F}^c = \sum_{j=1}^{n_p} x_{cj} \rho_j \mathbf{u}_j + s_j \rho_j \mathbf{J}_{cj}, \quad c = 1, \dots, n_c. \quad (3)$$

Here the velocity \mathbf{u}_j follows the extension of Darcy's law to multiphase flow,

$$\mathbf{u}_j = -\mathbf{K} \frac{k_{rj}}{\mu_j} (\nabla p_j - \gamma_j \nabla z), \quad (4)$$

where \mathbf{K} is the permeability tensor (mD), k_{rj} is the relative permeability of phase j , μ_j is the viscosity of phase j (mPa s), p_j is the pressure of phase j (bar), $\gamma_j = \rho_j g$ is the specific weight (N/m^3) and z is the depth (m). The \mathbf{J}_{cj} is the diffusion flux of component c in phase j , which is described by Fick's law as

$$\mathbf{J}_{cj} = -\phi \mathbf{D}_{cj} \nabla x_{cj}, \quad (5)$$

where \mathbf{D}_{cj} is the tensor of diffusion coefficients (m^2/day).

The governing equations are discretized using the finite volume approximation and fully implicit method. The resulting system of algebraic equations is highly nonlinear and it is linearized using the Operator-Based Linearization (OBL) approach (Voskov 2017). This approach significantly simplifies the implementation of the simulation framework by introducing algebraic operators that capture all complex physics and nonlinear terms. The physical terms in the conservation equations are separated into thermodynamic state-dependent and discretization-dependent operators. The state-dependent operators are parameterized in the physical space and during the course of a simulation, they are evaluated by multi-linear interpolation. Moreover, the derivatives required for the assembly of the linear system are readily obtained through the interpolation coefficients. In this work, we utilize the formulation of mass balances from Lyu et al. (2021) which was later generalized in Lyu and Voskov (2023).

2.2 Physical Properties

We consider a binary system with H_2O and CO_2 that distributes between a vapor and an aqueous phase in which the effect of salinity is neglected. A fugacity-activity approach

is applied to a negative flash procedure with successive substitution (Michelsen and Mollerup 2007). For the vapor phase, fugacities are evaluated from the Peng-Robinson equation of state (Peng and Robinson 1976), and for the aqueous phase, an activity model is used (Ziabakhsh-Ganji and Kooi 2012). The results of this approach and properties of the separate fluid phases at atmospheric conditions are displayed in Fig. 1. In addition, the figure shows density and viscosity models for CO₂-saturated brine and the gas mixture at atmospheric conditions in comparison with experimental data. A remark on the use of the OBL technique under these conditions; with the low solubility of CO₂ in water, it is crucial to apply an OBL resolution that is sufficiently fine to capture the solubility limit of CO₂ in brine (Lyu and Voskov 2023).

For capillary pressure curves, data on entry pressures at residual water saturation were provided for the different sand facies. The model response is extremely sensitive to capillary pressure curves, as the injected gas rapidly migrates upwards due to large density differences, leading to low gas saturation reaching the capillary barrier. The coarse resolution of the grid is then unable to impose the capillary trapping mechanism, leading to a CO₂ plume that is crossing the capillary barriers. In our initial submission, we applied a constant capillary pressure function, equal to the reported values of entry pressure in Nordbotten et al. (2022) and we keep the same strategy in this study.

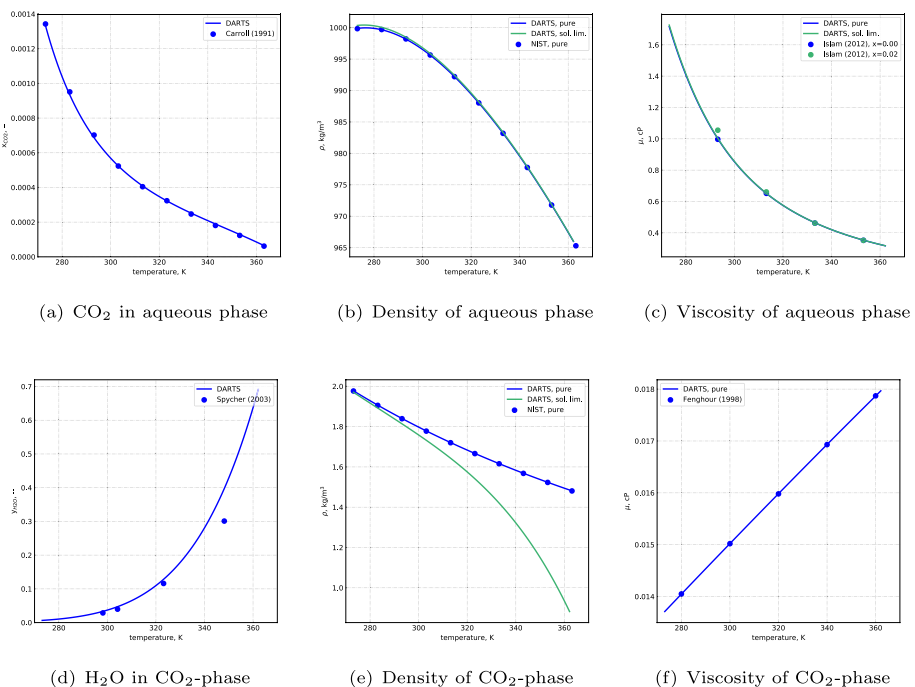


Fig. 1 Phase properties of aqueous phase (upper) and CO₂-rich phase (lower) at atmospheric pressure ($p = 1.01325$ bar). **a** Solubility of CO₂ in the aqueous phase and **d** H₂O in the CO₂-phase, **b** brine density (Spivey et al. 2004; Garcia 2001) and **e** CO₂-phase density (Peng and Robinson 1976), **c** brine viscosity (Islam and Carlson 2012) and **f** CO₂-phase viscosity (Fenghour et al. 1998). Blue lines for density and viscosity are pure phase properties, green lines are saturated phase properties. Data from Carroll et al. (1991); Spycher et al. (2003); Lemmon et al. (2022); Islam and Carlson (2012)

Lastly, diffusion is an important driver behind gravitational instabilities at the interface between CO₂-saturated brine and pure brine, followed by the development of density-driven fingering. Consequently, diffusion coefficients are a determining factor for finger onset time and wavelength (Riaz et al. 2006) (see also Appendix 1). However, data on binary diffusion coefficients for CO₂ and water in the aqueous phase under atmospheric conditions are not well studied. We included the uncertainties around reported binary diffusion coefficients into the uncertainty quantification, described in Sect. 2.4.

2.3 Computational Grid

The FluidFlower rig comprises a heterogeneous sand pack assembled within a thin, slightly curved filled Hele-Shaw cell of 2.8 m wide by 1.3 m high. A digitized version of the geometry, displayed in Fig. 2, constructed from high-resolution images in Nordbotten et al. (2022), contains the coordinate data. The setup contained variations in thickness from the intended constant 25 mm, as reported by the experimental group. The boundaries of the rig are closed on the bottom, left, and right sides, and the top is open and in contact with the atmosphere, with a free water table at a fixed level.

The rig has been filled with six different sand types, from finest to coarsest labeled as ESF, C, D, E, F, and G, subdivided into four regions with specific Corey-related parameters. In addition, we accounted for the anisotropy in some layers (ESF, C, and D) for which internal layering, due to the manual filling of the rig, is observable in the images. The properties of the separate layer types are estimated through a history matching procedure and the uncertainty quantification described in Sect. 2.4. Finally, two ports for CO₂ injection, referred to as I1 and I2, are installed in the reservoir. The location of the injection ports, as well as that of two pressure sensors and three boxes, which are related to the comparison metrics related to CO₂ distribution used in the benchmark study, are marked in Fig. 2. During the experimental runs, CO₂ was injected from the first injection port for 5:00 h at a constant rate of 10 mL/min; injection from the second well starts after a 2:15 h delay and runs for 2:45 h, at the same volumetric rate.

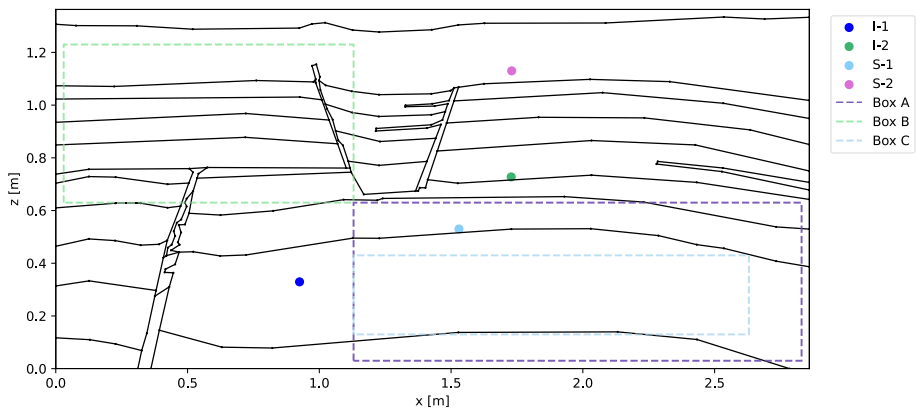


Fig. 2 Digitized FluidFlower geometry. High-resolution images and layer labeling are presented in Nordbotten et al. (2022). *I* refers to injection ports, *S* refers to pressure sensors and the boxes are used in the reporting of various comparison metrics

From the digitized geometry, we generated unstructured grids of different resolutions, with refinement around the well locations. A thickness correction was applied to the unstructured mesh according to a spline interpolation of the provided thickness map in the benchmark description. The constant pressure boundary condition at the top was mimicked by placing a production well connected to the top cells at atmospheric pressure.

2.4 Modeling Choices and Original Benchmark Submission

One of the aims of the benchmark study was to assess the predictive capabilities of the reservoir simulation community. The workflow we put up for making such predictions was threefold. From the tracer test data provided by the experimental group, we performed a history-matching procedure in order to populate the different sand facies with permeabilities and anisotropy (Tian et al. 2023). Then, a most representative model run, with best estimates of physical properties and (relatively) fine resolution, had to be defined and reported through a series of spatial distributions and other metrics over the course of the simulation, and finally, an estimate of the uncertainty around the reported metrics had to be given.

For the forward modeling, we considered three resolutions of the unstructured grids of approximately 14,000, 45,000, and 100,000 degrees of freedom (DOFs), respectively. Taking into account the prohibitive runtime of the finest grid, we took the intermediate resolution as a trade-off between the resolution and performance. According to analytic evaluation (see Appendix 1 for details), our discretization is not fully resolving the analytic wavelength of the first unstable mode which means that our results cannot be considered as numerically converged. For the purpose of quantifying the uncertainty, we performed a series of model runs with varying input for the most uncertain of all parameters, as summarized in Table 1. The permeabilities for each layer have been history matched based on the tracer test experiments; see details in Tian et al. (2023).

The results of a limited uncertainty quantification with only 100 realizations can be seen in Fig. 3. Here we show the dissolution of CO₂ in boxes A and B defined in Fig. 2 with P10, P50, and P90 quantiles for the dissolution in box A. A corresponding CO₂ concentration can be seen in Fig. 4 after 24, 48, and 72 h of simulation. You can clearly see that the character of CO₂ propagation and dissolution strongly depends on the variation of physical parameters assumed for the simulation. Besides, you can see a backward correlation between boxes A and B: the more CO₂ dissolves in box A the less it dissolves in box B. However, the dissolution of CO₂ in box B is almost an order of magnitude lower compared to box A due to the complex buoyancy-driven propagation of CO₂ into box B along the fault.

In our initial submission, we encountered some other relevant numerical issues. We used a two-point flux approximation (TPFA) with upstream weighting. Since the numerical scheme based on TPFA is inconsistent for non-K orthogonal unstructured grids, we considered Cartesian grids. These grids are K-orthogonal by definition but not suitable for capturing the complex geometry of the FluidFlower rig. A multi-point flux approximation (MPFA) is a fully consistent choice for an unstructured grid. However, MPFA is usually more expensive to solve

Table 1 Ranges for input parameters in uncertainty quantification

Parameters	Units	Distribution	Mean	Std
Temperature (T)	°C	Normal	23	2
Diffusion coefficient (D)	m ² / s	Log-normal	7 · 10 ⁻¹⁰	5 · 10 ⁻¹⁰
Corey parameters	–	Normal	See Table 2	5–50 %

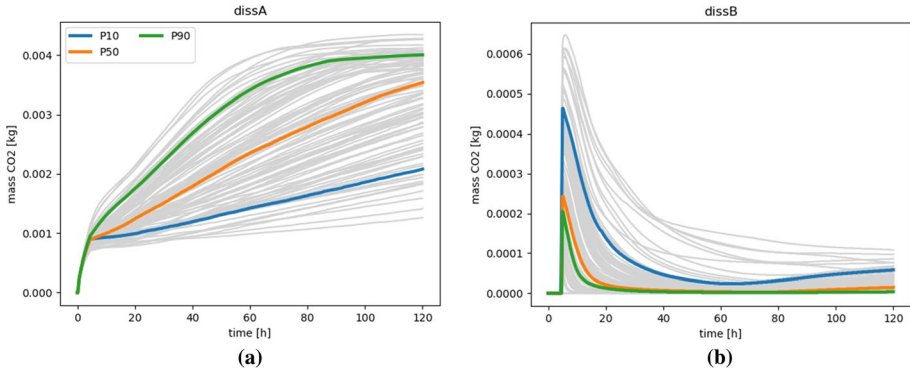


Fig. 3 CO₂ dissolution in box A (a) and box B (b) for 100 realizations with P10, P50, and P90 quantiles

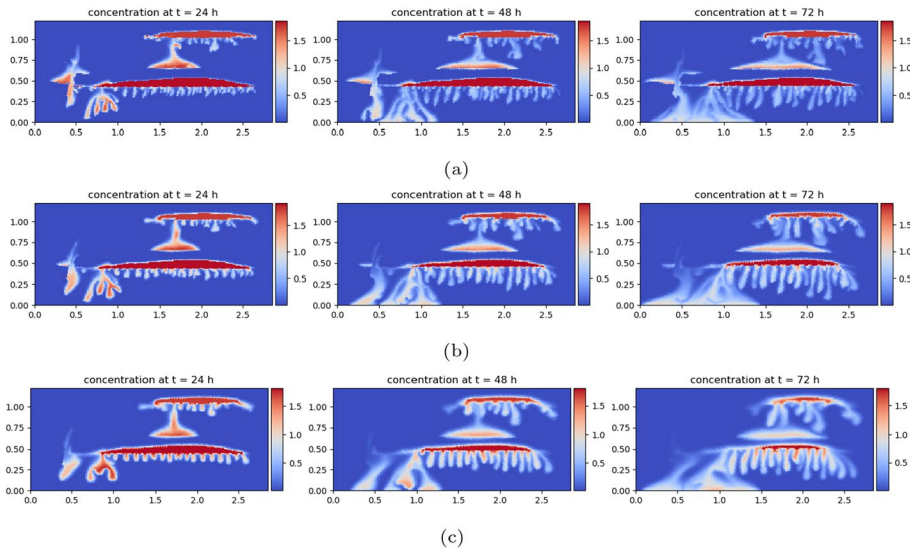


Fig. 4 Concentration of CO₂ for P10 (a), P50 (b), and P90 (c) realizations at 24, 48, and 72 h in simulation

and can significantly add to the already prohibitive time of the simulation. In addition, performing simulations under the atmospheric benchmark conditions required us to adjust our linear solver and time-step strategies. More discussion on discretization and solver issues follows in later sections.

2.5 Baseline Model and Metrics for Comparison Study

To address the effect of discretization in this comparison study (resolution, Cartesian/unstructured grid, approximation of the fluxes), a baseline model is established. In this version, a few simplifications have been made compared to the geometries and petrophysical properties used in our original submission. We use the layer properties reported in Table 2. Furthermore, the rig is assumed to be of a constant thickness with

no curvature and the injection ports consist of a well perforating the cell at the location reported in the benchmark description, contrary to our cylindrical well treatment in the original submission. The aim of this part of this study is primarily to investigate the effects of different gridding strategies, so any differences in outcomes between our contributions to the main simulation study and this baseline model are not a topic of discussion.

To compare the output of the different discretizations, we use a subset of the comparison metrics used in the main FluidFlower study (Flemisch et al. 2023): spatial distributions of gas saturation and CO₂ concentration in the brine were reported every 24 h on a uniform grid consisting of 1 cm by 1 cm cells, and dense time series recorded accumulation of CO₂ in different forms (free gas and dissolved) in boxes A and B (see Fig. 2) in 10-minute intervals.

3 Solver and Time-Step Strategies

The nonlinear solver in DARTS is based on the Newton–Raphson method and required the linearization of the original system of governing equations described by (1). The Jacobian assembly for the isothermal model requires a connection list, pore volumes, and initial reservoir state. For the thermal model, extra arrays for rock heat capacity and conduction are also required. In addition, the interpolation of operator values and derivatives should be applied as a preparatory step before Jacobian assembly which is performed based on vectorized interpolators. The interpolation is performed within the existing points in the parameter space of the physical problem and new points are generated adaptively on demand (Khait and Voskov 2018).

The linear solution of system (1) is implemented based on direct or iterative linear solvers. For the direct linear solver, DARTS uses the SUPERLU library (Grigori et al. 2007). The main iterative solver is the flexible generalized minimum residual (FGMRES) iterative method (Saad 1993) with constrained pressure residual (CPR) preconditioner (Wallis 1983; Wallis et al. 1985). The CPR preconditioner includes two stages where at the first stage, the True-IMPES reduction to pressure equation produces an elliptic-like system solved with a single V-cycle of AMG solver. The second stage includes an ILU(0) preconditioner for the remaining hyperbolic-like part of the linear system. Both Jacobian assemble and iterative linear solver are implemented on both CPU and GPU platforms (Khait et al. 2020).

To improve the nonlinear convergence in the case of benchmark conditions, we also propose a special heuristic for the timestep choice. The conventional treatment of timestep

Table 2 Porosity, permeability and petrophysical properties for different sand types

Type	$\phi(-)$	$k(D)$	$n_w(-)$	$n_g(-)$	$s_{wc}(-)$	$s_{gc}(-)$	$k_{rwe}(-)$	$k_{rge}(-)$	$p_e(mbar)$	$k_z/k_x(-)$
ESF	0.43	44	2.0	1.5	0.11	0.06	0.80	0.85	15	0.75
C	0.44	473	2.0	1.5	0.12	0.08	0.93	0.95	3	0.8
D	0.44	1110	2.0	1.5	0.14	0.10	0.93	0.95	1	0.9
E	0.45	2005	2.0	1.5	0.32	0.14	0.71	0.75	–	1.0
F	0.45	4259	,	,	,	,	,	,	–	,
G	0.44	9580	,	,	,	,	,	,	–	,

in reservoir simulation is based on starting with a relatively small timestep to fully resolve the initial transient regime and potential non-equilibrium initialization. In the process of simulation, the timestep is multiplied by a certain factor if nonlinear iterations converge in a predefined number of iterations or divided by this factor if not. When the simulation reaches a maximum predefined timestep, it will be used for the rest of the simulation assuming nonlinear iterations are convergent. Some heuristics usually enhance this strategy with sensitivity to variable changes, nonlinear convergence, and time truncation error (Aziz and Settari 1979).

Together with the linear update at every nonlinear iteration provided by the Newton–Raphson approach, the nonlinear solver in DARTS includes a simple timestep strategy and local and global chop of governing unknowns to preserve the convergence. For the benchmark, we adjusted the default timestep strategy and added the following heuristic:

- The ultimate maximum timestep in simulation is defined as equal to 1 min.
- Dynamic maximum timestep is adjusted based on the number of converged or failed nonlinear iterations in a certain time period (reporting time). For example, if the number of nonlinear iterations remains below 5 for more than 20 timesteps, the maximum timestep size will be doubled.
- In case there are more than 5 timestep cuts due to the non-converged iterations (with the maximum number of nonlinear iterations defined as 10), the maximum timestep will be reduced by a factor of 4.
- If L_∞ normalized residual in the nonlinear update violates the limit of 10^6 or if the same residual is repeated in the same gridblock more than 3 times, the timestep will be cut.

This simple heuristic in the customized nonlinear solver allowed us to improve the simulation CPU by a factor of 2–3 times (depending on the resolution) in comparison with the conventional simulation strategy.

The default nonlinear strategy in DARTS proves its robustness for a wide range of industrial applications at reservoir conditions. However, for the FluidFlower benchmark, our default strategy failed mostly due to the linear preconditioner. Soon, after the simulation reaches the post-injection period, the iterative linear solution reaches the maximum number of iterations which indicates the failure of the CPR preconditioner. This behavior has been reported by most teams during benchmark exercises and we link it to the large difference between the scaling of equations representing brine and CO_2 . Notice that the surface conditions change the ratio between Jacobian entries representing derivatives of conservation equation for gas and brine in respect to pressure by almost 3 orders of magnitude due to the changes in density and viscosity.

To illustrate the convergence issues at surface conditions, we run a coarse benchmark model using the iterative linear solver with CPR preconditioner in two regimes:

- At benchmark condition $p = 1$ bar and $T = 293$ K,
- And at real reservoir condition $p = 100$ bar and $T = 320$ K.

The statistics for two runs are shown in Table 3. Notice that the number of linear iterations was limited by $N_l = 200$ and it was hit 766 times in the simulation at benchmark conditions while it was only reached 18 times in the simulation at reservoir conditions. As a result, while the simulator performs more timesteps (TS) and nonlinear iterations (NI) for reservoir conditions, there are twice more linear iterations per nonlinear iteration (LI/NI) for converged timesteps at surface conditions and about four times more wasted

Table 3 Parameters of simulation runs

Test case	TS (wasted)	NI (wasted)	LI/NI (wasted)	LI > 200	CPU, sec
Benchmark conditions	19,610 (484)	25,492 (4,237)	26 (66)	766	2664
Reservoir conditions	34,534 (814)	67,023 (7,523)	12 (16)	18	2597

Table 4 Grids and resolutions for comparison

Resolution	Grid type	Mesh, m	# DOF
Coarse	Cartesian	0.019×0.018	11,250
Fine	Cartesian	0.0095×0.0091	45,000
Coarse	Unstructured	0.03	11,250
Fine	Unstructured	0.015	47,731

timesteps. This comparison quite clearly demonstrates that the conventional linear/nonlinear strategy in practical reservoir simulation is significantly challenged by runs in benchmark conditions.

4 Effects of Discretization

In this section, we discuss different discretization techniques and compare them. First, a comparison between Cartesian and unstructured grids, with approximately the same number of DOFs, and sensitivity to grid resolution is assessed, with regard to the benchmark's spatial and temporal reporting metrics. Following, the implications of two-point and multi-point flux approximations are investigated.

4.1 Cartesian Versus Unstructured Gridding

While Cartesian grids are often used in enhanced dissolution studies with certain convergence in the numerical results achieved (Elenius et al. 2015), it is still unclear how the structured nature of the grid affects the numerical results of enhanced dissolution problems. From one side, two-point flux approximation (TPFA) applied on a structured grid is fully consistent and K-orthogonal. However, a structured grid introduces a strong orientation grid effect which may in turn affect the numerical results.

We compare Cartesian and unstructured gridding using the conventional TPFA at different resolutions. We use the baseline grid with characteristic mesh size and a number of grid cells shown in Table 4, such that the number of degrees of freedom at the two resolutions is comparable. Finer resolution demonstrates a prohibitive run time and we decided to not include it in this study. It must be noted that, for all unstructured models, we keep a locally refined mesh near injection ports with a characteristic mesh size of 0.003 m. The Cartesian grids do not have this refinement.

The results for simulation after 1 day and 5 days on the unstructured and Cartesian grids for coarse and fine resolutions are shown in Fig. 5. It can be observed that on the unstructured grids, the coarse resolution is not able to capture the distribution from the fine

grid, the CO_2 plume extending less far into the domain. Remarkably, the final distribution of CO_2 for the fine resolution resembles more closely the outcomes of the experimental runs, although we assumed a constant thickness for this setup as opposed to our efforts in the main benchmark where a variable thickness has been applied. On Cartesian grids, the distribution of CO_2 deviates significantly from the results obtained on unstructured grids and from reported experimental outcomes. Coarse and fine resolutions show similar spatial distributions and a much finer resolution is required to converge to accurate results (see Appendix 1 for details).

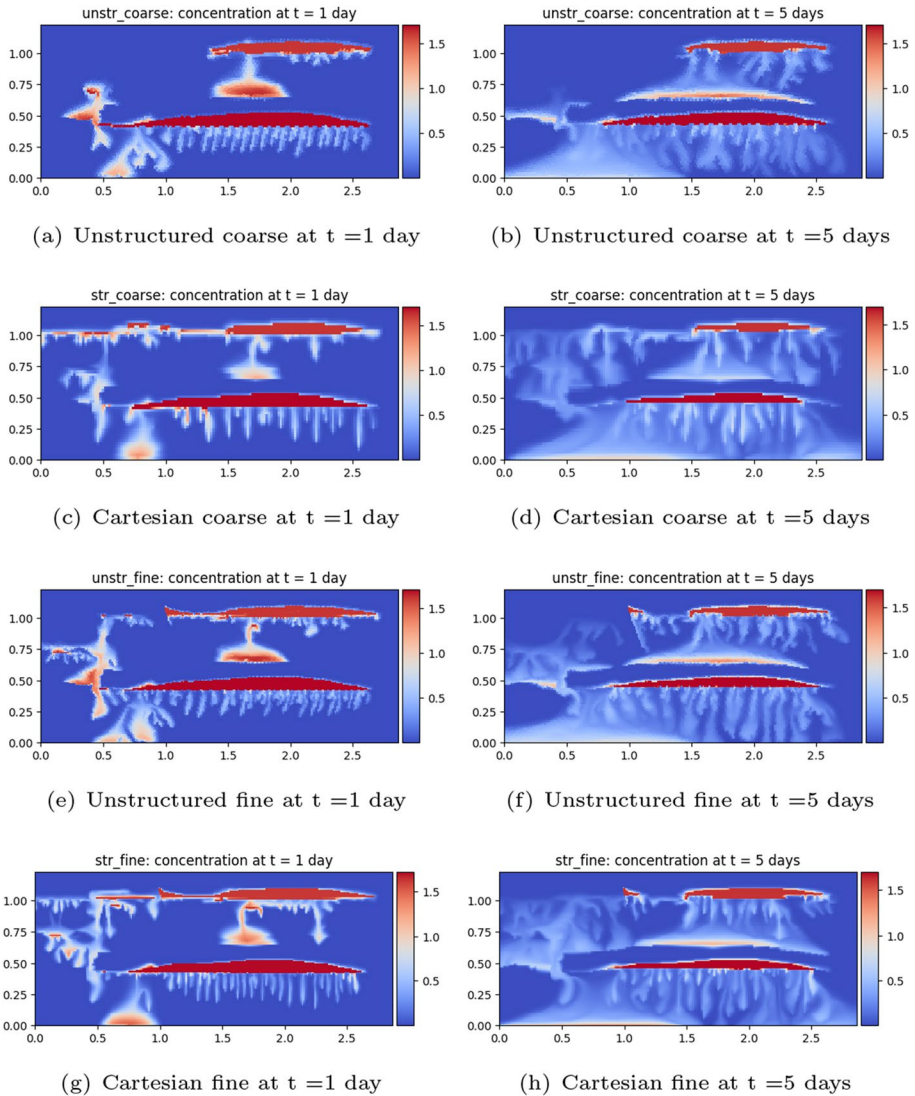


Fig. 5 Spatial distribution of CO_2 concentration in brine (kg/m^3) on unstructured and Cartesian grids for coarse and fine resolutions, at $t = 1$ day and $t = 5$ days

Another source of differences between unstructured and Cartesian grids is the pattern of gravity-driven fingers. On the unstructured meshes, the onset time of convective mixing and the wavelength of the fingers show less sensitivity to the resolution. On the other hand, there exists a notable difference in fingering patterns between coarse and fine resolutions for the Cartesian grids, which is most evident in wavelength.

In Fig. 6, the temporal evolution of the total quantities of CO₂ in different forms (free gas and dissolved in brine) in Boxes A and B are shown. The amounts of CO₂ accumulating in both boxes is often higher in the structured models. Furthermore, the inflow and outflow of CO₂, either through flow or dissolution of free gas into the brine, exhibits a smooth pattern in unstructured grids, while it is much less smooth in structured ones. This resembles the grid-dependent numerical effect reported by some groups that used a Cartesian grid in the benchmark study when the water-gas contact coincides with cell faces and bursts the dissolution (Flemisch et al. 2023).

It is obvious that the significant differences in spatial and temporal quantities in the results arise from several factors. They include gridding type, mesh resolution, and thickness of the rig for the benchmark problem. That explains a significant divergence of reported values between different groups in the main simulation benchmark. Notice that these results do not even consider uncertainties in the physical modeling.

4.2 Two-Point Versus Multi-Point Flux Approximation

As discussed in the previous section, the modeling on structured grids used in this paper may suffer from the grid orientation effect which can affect fingering and the resulting amount of CO₂ trapped. On the other hand, the unstructured grids are not fully K-orthogonal which makes the numerical scheme based on two-point flux approximation

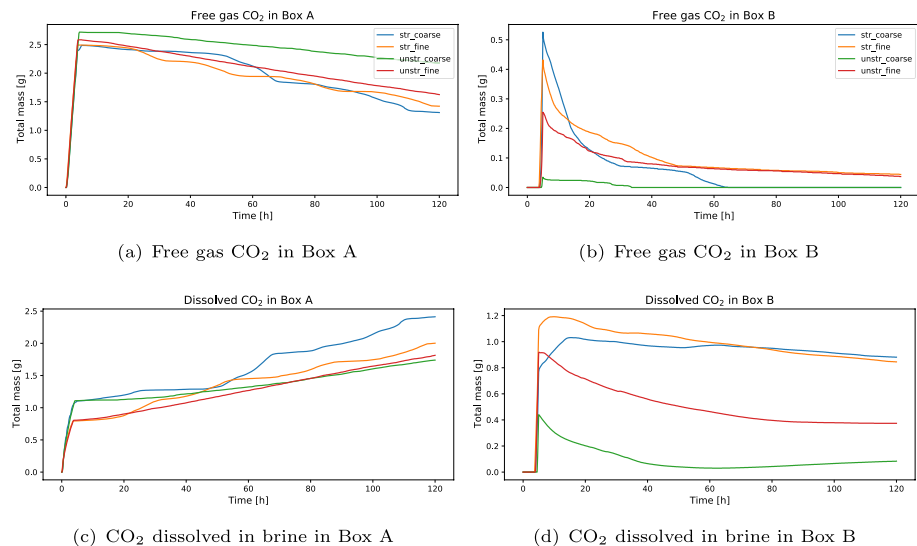


Fig. 6 Evolution of total mass (g) of free gas CO₂ and CO₂ dissolved in brine in Box A (left) and Box B (right) for Cartesian and unstructured grids for coarse and fine resolutions over time

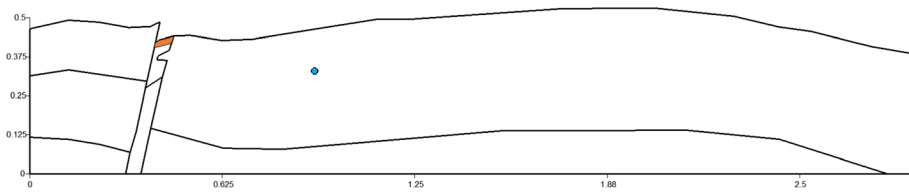


Fig. 7 A cut of FluidFlow geometry. The injection well is located inside the blue circle while the production well is placed in the orange rectangle

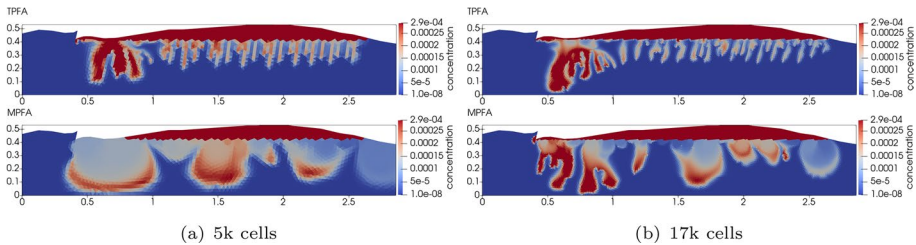


Fig. 8 Resolution study for the model cut in benchmark conditions. The comparison of the spatial distributions of CO_2 concentration after 24 h was obtained with TPFA and MPFA schemes

(TPFA) inconsistent for these grids. To investigate the fingering process against these issues we perform a simulation with multi-point flux approximation (MPFA).

We run a simulation for the lower part of the benchmark geometry where the most of fingering is observed. The model geometry is shown in Fig. 7. We place a sink at the top of the most permeable layer to keep the same flow pattern as in the original geometry. The constant pressure is maintained at the sink while the injector is working under the constant injection rate same as in the benchmark. We use a gradient-based variant of the averagely weighted linear MPFA scheme (Vassilevski et al. 2020) which is sometimes called AvgMPFA (Schneider et al. 2018). Both fluid flux and component diffusion are treated with AvgMPFA.

Figure 8 shows results obtained in the benchmark conditions. It can be seen that the MPFA scheme demonstrates a larger wavelength of the fingers very different from TPFA results and experimental observations. In-depth investigations of this behavior indicate that the non-locality of MPFA stencil expands the influence of small pressure perturbations in the model that ignites wider perturbations in concentrations and reflects in larger fingers. This effect is reduced with the resolution but is still significantly present at benchmark conditions.

To make consistent comparisons in more practical reservoir conditions, we scaled porosity, permeabilities, capillary pressure, and injection rates to in-situ conditions of typical subsurface aquifers. The corresponding parameters for each layer are specified in Table 5. Pressure and temperature have been scaled to $p = 100$ bar and $T = 320$ K similar to the linear solver comparison. Due to the different parameters of sand and fluids, the onset time becomes larger and simulation results are shown after 15 days.

Figure 9 shows the results of the simulation for these conditions. Here, local perturbations in pressure are reflected in lower velocities which reduce the fluctuations present in MPFA discretization for benchmark conditions. That can be explained by a several times larger gradient in concentration for surface conditions which in combination with a larger

Table 5 Absolute permeabilities, porosities and entry pressures for modeling

Facies	Index l	k (D)	$\phi(-)$	p_e (bar)
ESF	1	0.5	0.18	0.1
C	2	1	0.2	0.03
D	3	5	0.22	0.01
E	4	20	0.25	0.0
F	5	1	0.2	0.0
G	6	20	0.25	0.0

stencil in discretization for pressure and composition creates instabilities with a larger wavelength in comparison with benchmark results. Moreover, differences between results using TPFA and MPFA discretizations for realistic reservoir conditions are significantly reduced. Both schemes demonstrate similar instabilities and corresponding enhanced dissolution rates.

It is also important to notice that while TPFA discretization is only valid for the K-orthogonal grid, the default gridding with wedges usually introduces a very limited number of non-orthogonal interfaces. In Fig. 10 we show the statistical analysis of the coarse and fine grids with the distribution of angles deviating from 90 degrees for the smaller model and for the full benchmark model. The angles are measured for every interface in the grid between a line connecting the centers of adjacent cells and a line connecting the cell center and the center of an interface between the cells. According to the figure, we observe a lower deviation from orthogonality for finer mesh with more than 90% of interfaces within a very little (less than 5 degrees) deviation from orthogonality, making TPFA quite applicable for the simulation. Besides, the explicit orthogonalization procedure suggested in Karimi-Fard (2008) can improve the orthogonality of unstructured grids even further.

5 Lessons Learned

The proposed simulation framework allowed efficient modeling of the FluidFlower experiment using advanced numerical techniques. The robust thermodynamic library allowed for accurate modeling of fluid properties at various conditions ranging from benchmark to reservoir states. The advanced linearization approach in combination with the robust nonlinear formulation provides an efficient fully implicit solution which is

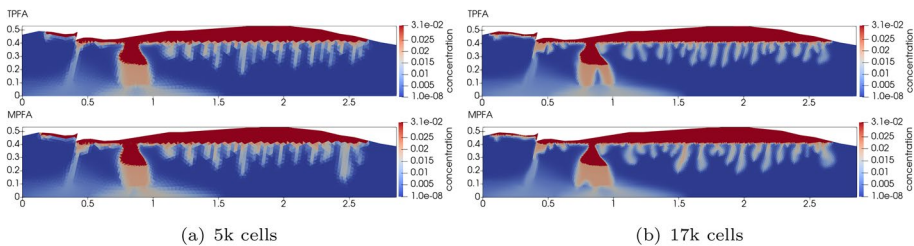


Fig. 9 Resolution study for the model cut in reservoir conditions. The comparison of the spatial distributions of CO₂ concentration after 15 days was obtained with TPFA and MPFA schemes

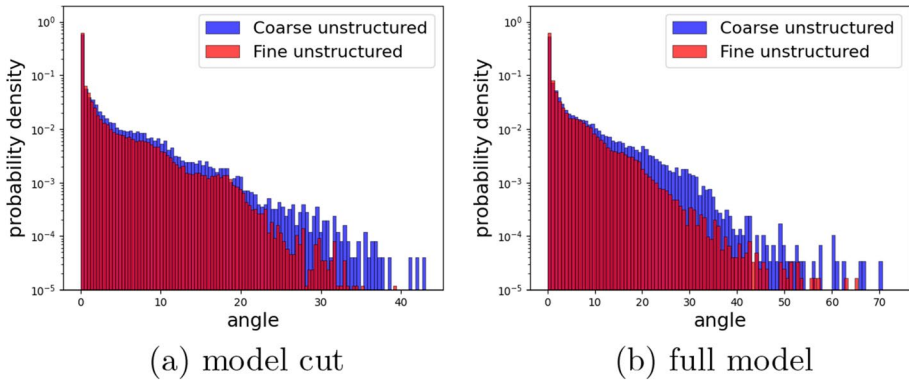


Fig. 10 Distribution density of angles deviated from orthogonality in log space plotted for the unstructured coarse and fine grids for the model cut (a) and for the full model (b). The angles are calculated for every interface in the grid between a line connecting the centers of adjacent cells and a line connecting the cell center and the center of an interface between the cells

extremely important for the evaluation of different uncertain conditions present in the FluidFlower benchmark study. Generic unstructured gridding allowed for flexibility in the representation of various important features present in the experimental setup starting from the layered heterogeneity and finishing with an approximation of injection ports.

The high nonlinearity of the benchmark model introduces computational challenges for both linear and nonlinear solvers. It results in timestep degradation and the use of local and global chops to preserve the convergence of the nonlinear solver. We used a heuristic timestep strategy to facilitate the pace of the simulation. The strategy is based on the adjustment of maximum timestep with the number of converged and failed nonlinear iterations. The failure of the CPR preconditioner for the benchmark conditions is a main factor significantly increasing the computational cost of benchmark simulation. In this study, we clearly demonstrate that this failure is directly related to the physical conditions of the benchmark study (a combination of pressure, temperature, and permeabilities) and not to the scale or geometry of the benchmark setup. While the main reason for such behavior can only be revealed by in-depth analysis of the corresponding linear matrices, we relate it with larger contrast between physical properties (mostly density and viscosity) between CO_2 and brine at reservoir and surface conditions.

A study on the resolution and comparison of unstructured and Cartesian gridding reveals a high sensitivity of the overall distribution of CO_2 throughout the domain to gridding choices. Based on these modeling decisions alone, large differences occur in the main benchmark's reporting metrics, especially for box B. Overall, the physical phenomena associated with the main trapping mechanisms for CO_2 sequestration can be captured relatively well. However, the wavelength of gravity-driven instabilities shows deviations between Cartesian grids of different resolutions. Furthermore, the shape of the fingers illustrates the grid orientation effect of the Cartesian grid, at least at early times. Concluding, it can be seen that the grid resolution plays quite an important role in FluidFlower modeling and the finer grid is needed for a fully numerically converged solution. This conclusion is also supported by an analytic evaluation of the first unstable wavelength mode at the benchmark parameters.

The use of MPFA for unstructured meshes allowed the grid orientation effect to be alleviated, keeping the consistency of approximation. However, the results obtained with MPFA demonstrate a remarkably higher wavelength of the fingers compared to the one observed in the experiment and in the TPFA modeling. The reasons for that are the higher gradient in concentration at benchmark conditions and the wider stencil of MPFA which expands the influence range of pressure perturbations and introduces non-physical fluctuations. At the same time, this mismatch is not observed in the modeling under realistic reservoir conditions where the gradient in concentration is reduced by almost 3 times. It may also indicate the different source of perturbation which is more pronounced under lower fluid velocities. This issue requires further investigation that goes beyond the scope of this paper.

In conclusion, it is quite obvious that the benchmark conditions pose new challenges to the conventional reservoir simulation technique mostly used for modeling of CO₂ sequestration at realistic subsurface conditions. While the benchmark conditions are primarily derived from analog laboratory experiments like FluidFlower, they can potentially manifest in practical CO₂ sequestration scenarios, such as the mineral trapping process in basaltic rock formations at shallow depths. Within our study, we have identified possible directions for analyzing this behavior. However, more effort should be put into a detailed investigation of these issues and developing innovative techniques to address and mitigate them effectively. By doing so, we can enhance our understanding of CO₂ sequestration and facilitate the development of more efficient and reliable methodologies in this field.

Appendix 1

Following the model proposed in Riaz et al. (2006); Elenius et al. (2014), the theoretical wavelength of the first unstable mode can be estimated using the following relation:

$$\lambda_c = \frac{2\pi\mu_w D\phi}{A_1 k \Delta\rho_w g}. \quad (6)$$

Following Riaz et al. (2006), the constant $A_1 = 0.07$ when the rest of the parameters are defined in the benchmark conditions as

- $\mu_w = 10^{-3}$ Pa s,
- $\Delta\rho_w = 0.3$ kg / m³,
- $D = 10^{-9}$ m² / s,
- $g = 9.8$ m / s²,
- $\phi = 0.45$,
- $k = 2 \cdot 10^{-10}$ m.

Using these parameters, the wavelength of instabilities is supposed to be around $\lambda_c = 7$ mm. The fine discretization models use slightly coarser grid resolution so our numerical results cannot be considered as fully converged yet.

Acknowledgements The open-darts project is supported by the Netherlands eScience Center under grant number NLESC.OEC.2021.026. We also want to acknowledge Artur Palha and Luisa Orozco for their contribution to the open-darts development.

Author Contributions All authors contributed to the study conception and design. The first draft of the manuscript was put together by DV and MW. MW contributed to the physical modeling and Cartesian/unstructured grid construction, XT prepared the set of realizations. AN prepared the comparison between TPFPA/MPFA and Denis Voskov worked on linear solver strategies. All authors read and approved the final manuscript.

Funding Author Michiel Wapperom received financial support from TotalEnergies; Xiaoming Tian China Scholarship Council (CSC). The authors have no relevant financial or non-financial interests to disclose.

Data Availability The source code for DARTS simulation framework used in this work can be found at <https://gitlab.com/open-darts>.

Declarations

Conflict of interest The authors have not disclosed any competing interests.

Open Access This article is licensed under a Creative Commons Attribution 4.0 International License, which permits use, sharing, adaptation, distribution and reproduction in any medium or format, as long as you give appropriate credit to the original author(s) and the source, provide a link to the Creative Commons licence, and indicate if changes were made. The images or other third party material in this article are included in the article's Creative Commons licence, unless indicated otherwise in a credit line to the material. If material is not included in the article's Creative Commons licence and your intended use is not permitted by statutory regulation or exceeds the permitted use, you will need to obtain permission directly from the copyright holder. To view a copy of this licence, visit <http://creativecommons.org/licenses/by/4.0/>.

References

- Ajayi, T., Awolayo, A., Gomes, J.S., Parra, H., Hu, J.: Large scale modeling and assessment of the feasibility of CO₂ storage onshore abu dhabi. *Energy* **185**, 653–670 (2019). <https://doi.org/10.1016/j.energy.2019.07.052>
- Aziz, K., Settari, T.: *Petroleum Reservoir Simulation*. Applied Science Publishers, London (1979)
- Carroll, J.J., Slupsky, J.D., Mather, A.E.: The solubility of carbon dioxide in water at low pressure. *J. Phys. Chem. Ref. Data* **20**, 1201–1209 (1991). <https://doi.org/10.1063/1.555900>
- Daniel, D., Riaz, A.: Effect of viscosity contrast on gravitationally unstable diffusive layers in porous media. *Phys. Fluids* (2014). <https://doi.org/10.1063/1.4900843>
- Delshad, M., Kong, X., Tavakoli, R., Hosseini, S.A., Wheeler, M.F.: Modeling and simulation of carbon sequestration at cranfield incorporating new physical models. *Int. J. Greenh. Gas Control* **18**, 463–473 (2013). <https://doi.org/10.1016/j.ijggc.2013.03.019>
- Elenius, M.T., Gasda, S.E.: Convective mixing in formations with horizontal barriers. *Adv. Water Resour.* **62**, 499–510 (2013). <https://doi.org/10.1016/j.advwatres.2013.10.010>
- Elenius, M.T., Nordbotten, J.M., Kalisch, H.: Convective mixing influenced by the capillary transition zone. *Comput. Geosci.* **18**(3–4), 417–431 (2014). <https://doi.org/10.1007/s10596-014-9415-1>
- Elenius, M.T., Voskov, D.V., Tchelepi, H.A.: Interactions between gravity currents and convective dissolution. *Adv. Water Resour.* **83**, 77–88 (2015). <https://doi.org/10.1016/j.advwatres.2015.05.006>
- Fan, Y., Durlafsky, L.J., Tchelepi, H.A.: A fully-coupled flow-reactive-transport formulation based on element conservation, with application to CO₂ storage simulations. *Adv. Water Resour.* **42**, 47–61 (2012). <https://doi.org/10.1016/j.advwatres.2012.03.012>
- Farajzadeh, R., Zitha, P.L.J., Bruining, J.: Enhanced mass transfer of CO₂ into water: experiment and modeling. *Ind. Eng. Chem. Res.* **48**(13), 6423–6431 (2009). <https://doi.org/10.1021/ie801521u>
- Farajzadeh, R., Ranganathan, P., Zitha, P.L.J., Bruining, J.: The effect of heterogeneity on the character of density-driven natural convection of CO₂ overlying a brine layer. *Adv. Water Resour.* **34**(3), 327–339 (2011). <https://doi.org/10.1016/j.advwatres.2010.12.012>
- Fenghour, A., Wakeham, W.A., Vesovic, V.: The viscosity of CO₂. *J. Phys. Chem. Ref. Data* **27**(1), 31–44 (1998). <https://doi.org/10.1063/1.556013>
- Flemisch, B., Nordbotten, J.M., Fernø, M., Juanes, R., Class, H., Delshad, M., Doster, F., Ennis-King, J., Franc, J., Geiger, S., Gläser, D., Green, C., Gunning, J., Hajibeygi, H., Jackson, S.J., Jammoul, M., Karra, S., Li, J., Matthäi, S.K., Miller, T., Shao, Q., Spurin, C., Stauffer, P., Tchelepi, H., Tian, X.,

- Viswanathan, H., Voskov, D., Wang, Y., Wapperom, M., Wheeler, M.F., Wilkins, A., Youssef, A.A., Zhang, Z.: The FluidFlower forecasting and validation study for the storage of CO₂. Transp. Porous Media, this S.I. (2023)
- Garcia, J.E.: Density of aqueous solutions of CO₂. Technical report, Lawrence Berkeley National Laboratory (2001). <https://doi.org/10.2172/790022>
- Ghorbani, Z., Riaz, A., Daniel, D.: Convective mixing in vertically-layered porous media: the linear regime and the onset of convection. *Phys. Fluids* (2017). <https://doi.org/10.1063/1.4996049>
- Grigori, L., Demmel, J.W., Li, X.S.: Parallel symbolic factorization for sparse lu with static pivoting. *SIAM J. Sci. Comput.* **29**(3), 1289–1314 (2007). <https://doi.org/10.1137/050638102>
- Hesse, M.A., Orr, F.M., Tchelepi, H.A.: Gravity currents with residual trapping. *J. Fluid Mech.* **611**, 35–60 (2008). <https://doi.org/10.1017/S002211200800219X>
- Islam, A.W., Carlson, E.S.: Viscosity models and effects of dissolved CO₂. *Energy Fuels* **26**, 5330–5336 (2012). <https://doi.org/10.1021/ef3006228>
- Juanes, R., MacMinn, C.W., Szulczewski, M.L.: The footprint of the CO₂ plume during carbon dioxide storage in saline aquifers: storage efficiency for capillary trapping at the basin scale. *Transp. Porous Media* **82**(1), 19–30 (2010). <https://doi.org/10.1007/s11242-009-9420-3>
- Karimi-Fard, M.: Grid optimization to improve orthogonality of two-point flux approximation for unstructured 3D fractured reservoirs. (2008). <https://doi.org/10.3997/2214-4609.20146380>
- Khait, M., Voskov, D.V.: Adaptive parameterization for solving of thermal/compositional nonlinear flow and transport with buoyancy. *SPE J.* **23**(02), 522–534 (2018). <https://doi.org/10.2118/182685-PA>
- Khait, M., Voskov, D.V., Zaydullin, R.: High performance framework for modelling of complex subsurface flow and transport applications. In: 17th European Conference on the Mathematics of Oil Recovery (2020). <https://doi.org/10.3997/2214-4609.202035188>
- Lemmon, E.W., Bell, I.H., Huber, M.L., McLinden, M.O.: Thermophysical properties of fluid systems. Nat. Inst. Stand. Technol. Gaithersburg (MD) (2022). <https://doi.org/10.18434/T4D303>
- Lyu, X., Voskov, D.: Advanced modeling of enhanced CO₂ dissolution trapping in saline aquifers. *Int. J. Greenh. Gas Control* **127**, 103907 (2023). <https://doi.org/10.1016/j.ijggc.2023.103907>
- Lyu, X., Khait, M., Voskov, D.: Operator-based linearization approach for modelling of multiphase flow with buoyancy and capillarity. *SPE J.* (2021). <https://doi.org/10.2118/205378-PA>
- Michelsen, M.L., Mollerup, J.M.: Thermodynamic Models: Fundamentals and Computational Aspects. Tie-Line Publications, Holte (2007)
- Neufeld, J.A., Hesse, M.A., Riaz, A., Hallworth, M.A., Tchelepi, H.A., Huppert, H.E.: Convective dissolution of carbon dioxide in saline aquifers. *Geophys. Res. Lett.* (2010). <https://doi.org/10.1029/2010GL044728>
- Nomeli, M.A., Tilton, N., Riaz, A.: A new model for the density of saturated solutions of CO₂-H₂O-NaCl in saline aquifers. *Int. J. Greenh. Gas Control* **31**, 192–204 (2014). <https://doi.org/10.1016/j.ijggc.2014.10.006>
- Nordbotten, J.M., Celia, M.A.: Similarity solutions for fluid injection into confined aquifers. *J. Fluid Mech.* **561**, 307–327 (2006). <https://doi.org/10.1017/S0022112006000802>
- Nordbotten, J.M., Flemisch, B., Gasda, S.E., Nilsen, H.M., Fan, Y., Pickup, G.E., Wiese, B., Celia, M.A., Dahle, H.K., Eigestad, G.T., Pruess, K.: Uncertainties in practical simulation of CO₂ storage. *Int. J. Greenh. Gas Control* **9**, 234–242 (2012). <https://doi.org/10.1016/j.ijggc.2012.03.007>
- Nordbotten, J.M., Fernø, M., Flemisch, B., Juanes, R., Jørgensen, M.: Final benchmark description: fluid-flower international benchmark study. (2022). <https://doi.org/10.5281/zenodo.6807102>
- Pau, G.S.H., Bell, J.B., Pruess, K., Almgren, A.S., Lijewski, M.J., Zhang, K.: High-resolution simulation and characterization of density-driven flow in CO₂ storage in saline aquifers. *Adv. Water Resour.* **33**(4), 443–455 (2010). <https://doi.org/10.1016/j.advwatres.2010.01.009>
- Peng, D.-Y., Robinson, D.B.: A new two-constant equation of state. *Ind. Eng. Chem. Fundam.* **15**(1), 59–64 (1976). <https://doi.org/10.1021/i160057a011>
- Pruess, K., Nordbotten, J.: Numerical simulation studies of the long-term evolution of a CO₂ plume in a saline aquifer with a sloping caprock. *Transp. Porous Media* **90**, 135–151 (2011). <https://doi.org/10.1007/s11242-011-9729-6>
- Riaz, A., Tchelepi, H.A.: Linear stability analysis of immiscible two-phase flow in porous media with capillary dispersion and density variation. *Phys. Fluids* **16**(12), 4727–4737 (2004). <https://doi.org/10.1063/1.1812511>
- Riaz, A., Hesse, M., Tchelepi, H.A., Orr, F.M., Jr.: Onset of convection in a gravitationally unstable diffusive boundary layer in porous media. *J. Fluid Mech.* **548**, 87–111 (2006). <https://doi.org/10.1017/S0022112005007494>

- Riaz, A., Hesse, M., Tchelepi, H.A., Orr, F.M., Jr.: Onset of convection in a gravitationally unstable diffusive boundary layer in porous media. *J. Fluid Mech.* **548**, 87–111 (2006). <https://doi.org/10.1017/S0022112005007494>
- Ringrose, P.: *How to Store CO₂ Underground: Insights from Early-mover CCS Projects*. Springer, Cham (2020). <https://doi.org/10.1007/978-3-030-33113-9>
- Saad, Y.: A flexible inner-outer preconditioned gmres algorithm. *SIAM J. Sci. Comput.* **14**(2), 461–469 (1993). <https://doi.org/10.1137/0914028>
- Schneider, M., Gläser, D., Flemisch, B., Helmig, R.: Comparison of finite-volume schemes for diffusion problems. *Oil Gas Sci. Technol.* (2018). <https://doi.org/10.2516/ogst/2018064>
- Shukla, P.R., Skea, J., Slade, R., Khouardjaj, A.A., Diemen, R., McCollum, D., Pathak, M., Some, S., Vyas, P., Fradera, R., Belkacemi, M., Hasija, A., Lisboa, G., Luz, S., (eds.), J.M.: *Ippc, 2022: Summary for policymakers*. In: *Climate Change 2022: Mitigation of Climate Change. Contribution of Working Group III to the Sixth Assessment Report of the Intergovernmental Panel on Climate Change* (2017) <https://doi.org/10.1017/9781009157926.001>
- Spivey, J.P., McCain, W.D., North, R.: Estimating density, formation volume factor, compressibility, methane solubility, and viscosity for oilfield brines at temperatures from 0 to 275°C, pressures to 200 mpa, and salinities to 5.7 mole/kg. *J. Can. Pet. Technol.* **43**(7), 52–61 (2004). <https://doi.org/10.2118/04-07-05>
- Spycher, N., Pruess, K., Ennis-King, J.: CO₂-H₂ O mixtures in the geological sequestration of CO₂, i. assessment and calculation of mutual solubilities from 12 to 100°C and up to 600 bar. *Geochimica Cosmochimica Acta* **67**(16), 3015–3031 (2003). [https://doi.org/10.1016/S0016-7037\(03\)00273-4](https://doi.org/10.1016/S0016-7037(03)00273-4)
- Tian, X., Wapperom, M., Gunning, J., Wilkins, S.J.A., Green, C., Ennis-King, J., Voskov, D.: A history matching study for the fluidflower benchmark project. *Transp. Porous Media* (2023)
- Vassilevski, Y., Terekhov, K., Nikitin, K., Kapyrin, I.: Parallel finite volume computation on general meshes, (2020). <https://doi.org/10.1007/978-3-030-47232-0>
- Voskov, D.V.: Operator-based linearization approach for modeling of multiphase multi-component flow in porous media. *J. Comput. Phys.* **337**, 275–288 (2017). <https://doi.org/10.1016/j.jcp.2017.02.041>
- Voskov, D.V., Henley, H., Lucia, A.: Fully compositional multi-scale reservoir simulation of various CO₂ sequestration mechanisms. *Comput. Chem. Eng.* **96**, 183–195 (2017). <https://doi.org/10.1016/j.compchemeng.2016.09.021>
- Wallis, J.: Incomplete gaussian elimination as a preconditioning for generalized conjugate gradient acceleration. In: *Proceedings of 7th SPE Symposium on Reservoir Simulation* (1983) <https://doi.org/10.2118/12265-MS>
- Wallis, J., Kendall, R., Little, T., Nolen, J.: Constrained residual acceleration of conjugate residual methods. In: *Proceedings of the 8th SPE Symposium on Reservoir Simulation* (1985) <https://doi.org/10.2118/13536-MS>
- Wang, Y., Vuik, C., Hajibeygi, H.: Analysis of hydrodynamic trapping interactions during full-cycle injection and migration of CO₂ in deep saline aquifers. *Adv. Water Resour.* (2022). <https://doi.org/10.1016/j.advwatres.2021.104073>
- Ziabakhsh-Ganji, Z., Kooi, H.: An equation of state for thermodynamic equilibrium of gas mixtures and brines to allow simulation of the effects of impurities in subsurface CO₂ storage. *Int. J. Greenh. Gas Control* **11S**, 21–34 (2012). <https://doi.org/10.1016/j.ijggc.2012.07.025>

Publisher's Note Springer Nature remains neutral with regard to jurisdictional claims in published maps and institutional affiliations.